



Triple stub circuit topology as simultaneous insertion phase, amplitude and impedance control circuit for phased array applications

M. Unlu¹ S. Demir² T. Akin²

¹Electronics and Telecommunication Engineering Department, Cankiri Caddesi, Cicek Sokak, No. 3, Ulos, Ankara 06030, Turkey

²Electrical and Electronics Engineering Department, Middle East Technical University (METU), ODTU EEMB, Inonu Bulvari, Cankaya, Ankara 06531, Turkey

E-mail: mehmetu@umich.edu

Abstract: This study shows that the well-known triple stub circuit topology can also be used for controlling the insertion phase and amplitude of a given signal simultaneously, as well as preserving its impedance transformation ability. The triple stub circuit topology, which is nothing but an extension of the conventional double stub loaded-line phase shifter, results in one more degree of freedom to its solution when it is solved for its insertion phase. This additional degree of freedom not only brings the impedance transformation ability, but also allows tuning the circuit into a resonator at the frequency of interest whose quality factor can also be adjusted. This result is employed for controlling the amplitude of the output signal to any desired level, which is achieved using only low-loss transmission lines and shown to be true for any non-zero transmission line losses. The measurements of the fabricated sample circuits verify that it is possible to control simultaneously the insertion phase between 0 and 360° and the amplitude from -0.8 to <-15 dB, whereas the input return loss is always kept better than -15 dB as an example of their impedance transformation capabilities.

1 Introduction

Phase shifters have been one of the crucial building blocks for microwave/millimetre wave electronic systems, one of which is the phased arrays [1, 2]. The phased arrays have been developed starting from the 1950s and 1960s, and these efforts have also triggered numerous attempts for the development of the phase shifters.

There are two types of electronically controlled phase shifters in general that have been presented up to date. These are ferrite [2] and electronic switch phase shifters. Electronic switch phase shifters that use digital phase shift steps can be basically categorised into four types [3, 4], which are switched line [5, 6], reflection [7, 8], loaded line [9, 10] and switched network [3, 11] phase shifters. All of these types have been investigated in detail from different aspects [3, 4, 9].

The loaded-line phase shifters [12–15] uses two pairs of lumped element admittances or stubs as loading elements, which are usually switched by diodes. Garver [3] explored the bandwidth considerations of the loaded-line phase shifters together with its derivations, where Atwater [15] presented an extensive theoretical and practical analysis, which also includes the effects of the transmission line losses. It is clearly stated in both of the works that the loading elements' admittances and characteristic impedance of the transmission line connecting the loading elements should be fixed for a

desired phased shift. It is also stated in [15] that the electrical length of the transmission line connecting the loading elements is not arbitrary; rather it is related to the relative values of the admittances of the loading elements. This inherently shows that there are actually no free variables for the solution of the circuit, which leaves no space for any additional functionality. Although it is possible to tune the input impedance of the circuit to some extent by reflecting a fraction of the input power, there are theoretical limits to its impedance transformation range, and hence, the additional functions that it can perform.

Triple stub circuit topology, on the other hand, is actually nothing but an extension of the conventional double stub loaded-line phase shifter. This topology is very well known for its ability for making impedance transformation theoretically to any impedance [16] and comes up with infinitely many solutions. Examples of triple stub circuit topology as reconfigurable impedance tuners have been presented lately, which have a wide range for impedance tuning in a wide frequency band [17–19]. However, this topology has not been analysed to its limits for any additional functions that it can simultaneously perform together with its impedance transformation ability.

This paper shows that the triple stub circuit topology can provide any desired insertion phase between 0 and 360°, whereas it can still transform any real impedance to any other real impedance, including the matched load, Z_0 . It is also

demonstrated that the flexibility in the electrical length of the connecting transmission line can be used for tuning the circuit so that it behaves like a tunable quality factor resonating circuit, and hence, allows changing the amplitude of the input signal selectively, theoretically without any lower limits. It should be mentioned here that the function described above can be achieved with any non-zero value of transmission line loss. As a result, the triple stub circuit topology can be used for simultaneous insertion phase, amplitude and impedance control, which, to the best of the authors' knowledge, is presented for the first time in the literature.

The possibility that makes the proposed idea truly exciting arises when the idea is combined with contemporary integrated circuit and micro-electro-mechanical systems (MEMS) technologies, transforming the triple stub circuit topology into a reconfigurable circuit. As the state-of-the-art technologies can provide very low-loss switching components, the triple stub circuit topology can be used in passive phased arrays as an all-purpose, reconfigurable controlling element, which allows the emergence of phased arrays with increased functionality and reduced complexity.

2 Analytical solution

In this section, the analytical solution of the triple stub circuit topology will be presented for the lossless case first. The solution will be then investigated for the low-loss case, which is followed by the examination of the amplitude control in the following section. Here, the general case for the input impedance control is considered which inherently covers the zero return loss case, that is, where input impedance is Z_0 .

2.1 Lossless case

Fig. 1 shows the schematic of a triple stub circuit topology. The circuit is composed of three open-circuited transmission line stubs and two transmission lines connecting these stubs. x, y, z and t represent the physical lengths of the transmission lines where jX, jY and jZ represent the normalised susceptances of the stubs with respect to Z_0 , which is the characteristic impedance of all of the transmission lines.

The circuit can be represented with its $ABCD$ parameters, which can be calculated by cascading the $ABCD$ parameters of the stubs and connecting transmission lines as given in (1):

$$\begin{bmatrix} A & B \\ C & D \end{bmatrix}_{TSC, lossless} = \begin{bmatrix} 1 & 0 \\ jX & 0 \end{bmatrix} \begin{bmatrix} U & jT \\ jT & U \end{bmatrix} \begin{bmatrix} 1 & 0 \\ jY & 0 \end{bmatrix} \times \begin{bmatrix} U & jT \\ jT & U \end{bmatrix} \begin{bmatrix} 1 & 0 \\ jZ & 0 \end{bmatrix} \quad (1)$$

where $T = \sin(\beta t), U = \cos(\beta t)$

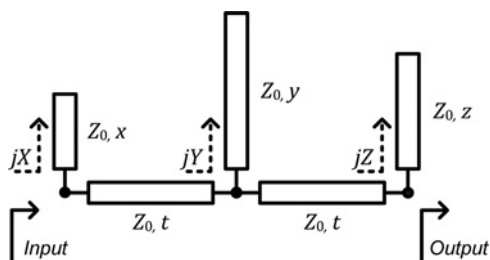


Fig. 1 Schematic of the triple stub circuit topology

The analysis starts with the selection of conditions for the impedance transformation and insertion phase control. The input impedance is assumed to be a real and positive number as expressed in (2), where S_{11} becomes as in (3)

$$Z_{in} = kZ_0, \quad k \text{ is real and positive} \quad (2)$$

$$S_{11} = \frac{k - 1}{k + 1} \quad (3)$$

Accordingly, the magnitude of S_{21} results as in (4), using the unitary property of lossless networks

$$S_{21} = |S_{21}| \angle S_{21} = \left(\frac{2\sqrt{k}}{k + 1} \right) \left(\frac{a + jb}{\sqrt{a^2 + b^2}} \right) \quad (4)$$

where $|S_{21}| = 2\sqrt{k}/(k + 1), \angle S_{21} = \arctan(b/a), a$ and b are real.

Controlling the insertion phase implies controlling the phase of S_{21} , and this is expressed by adding an arbitrary complex number of unity magnitude to the right hand side of (4).

Writing S_{21} in terms of the $ABCD$ parameters as in (5) and separating it into its real and imaginary parts yields two complex equations with four unknowns, which are X, Y, U and T

$$S_{21} = \frac{2}{A + B + C + D} = \left(\frac{2\sqrt{k}}{k + 1} \right) \left(\frac{a + jb}{\sqrt{a^2 + b^2}} \right) \quad (5)$$

$$S_{11} = \frac{A + B - C - D}{A + B + C + D} = \frac{k - 1}{k + 1} \quad (6)$$

Solving these equations, Y and Z can be found as in (7) and (8). Substituting the results of (7) and (8) into the imaginary part of (6) and solving for X gives (9). Using (7)–(9), one can find the susceptances, X, Y and Z , required for the desired phase shift. The stub lengths, x, y and z , can be easily found using the inverse trigonometric functions as in (10), where β is the wave number.

$$Y = \frac{1}{T^2} \frac{\sqrt{kb} + 2TU\sqrt{a^2 + b^2}}{\sqrt{a^2 + b^2}} \quad (7)$$

$$Z = \frac{1}{\sqrt{kb}T} \left(\sqrt{ka}T + \sqrt{kb}U + T\sqrt{a^2 + b^2} \right) \quad (8)$$

$$X = \frac{1}{kbT} \left(aT + kbU + \sqrt{k}T\sqrt{a^2 + b^2} \right) \quad (9)$$

$$\begin{aligned} X &= \tan(\beta x), Y = \tan(\beta y), Z = \tan(\beta z), T = \sin(\beta t), \\ U &= \cos(\beta t) \end{aligned} \quad (10)$$

It is observed from (7)–(9) that the stub lengths are dependent upon the selected insertion phase value and U and T , which are the functions of the length, t , of the connecting transmission lines. It also shows that the electrical length of the connecting lines is a free variable.

To verify the validity of the solution, a case study is carried out for a fixed electrical length of the connecting transmission lines, $t = \lambda/8$, which is a common choice for stub-based circuits. At this point, k is set to 1 to obtain a perfectly matched circuit, that is, where $S_{11} = 0$. This circuit is simulated using Microwave Office [20] at a centre

frequency of 15 GHz in 0–360° range with 1° steps, where the lengths of the stubs are calculated using (7)–(10). The effective permittivity of the transmission lines, $\epsilon_{r, \text{eff}}$, is selected as 1 during the simulations. Fig. 2 shows that the formulation works well for 0–360° using lossless lines (black line with circles).

2.2 Effects of the transmission line losses

To see the possible effects of the transmission line losses, the circuit is simulated again by adding the attenuation constants to the model and without changing any other parameters, where the lengths of the stubs are again calculated using (7)–(10). The simulation results are given in Fig. 2 for two different attenuation constants, $\alpha = 2$ and 5 Np/m at the centre design frequency, 15 GHz.

Examining the simulation results, one can see that the losses become effective and the insertion loss of the circuit starts to increase. The magnitude of S_{21} is better than –3 dB when the circuit is set for 42–337° and 86–326° insertion phase ranges for $\alpha = 2$ and 5 Np/m, respectively. Out of these ranges, the circuit suffers from the losses, which is because of the deteriorating return losses that become worse than about –12 dB. However, thanks to the solution provided above that has one free variable, t , 0–360° range can be easily covered by tuning t . Once the circuit is employed as a phase shifter, one can always find a t value, for which a low-insertion loss region can be obtained. Fig. 3 shows the performance of the circuit for different values of t . For all of the cases in the figure, return loss is as good as that of $t = \lambda/8$ case.

3 Amplitude control method

It was analytically proven in Section 2 that the insertion phase of the triple stub circuit topology can be controlled, whereas its input impedance is transformed to any real impedance. In addition, the circuit can also be used for adjusting the amplitude of the input signal together with the above mentioned properties, and the amplitude of the signal can be tuned practically as much as 15 dB.

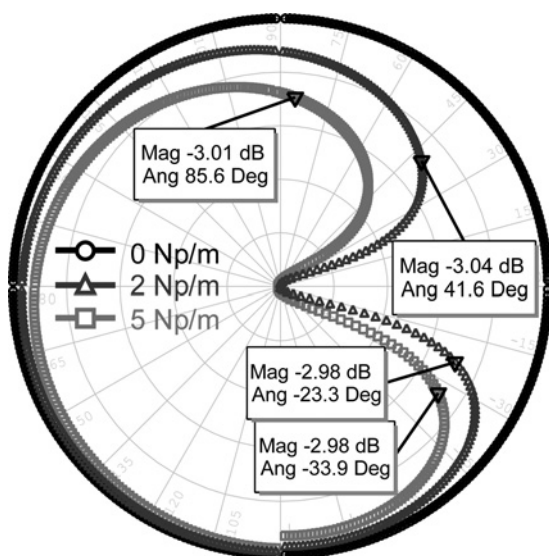


Fig. 2 Simulated S parameters of the triple stub circuit topology with respect to the desired insertion phase ($t = \lambda/8$ @ 15 GHz)

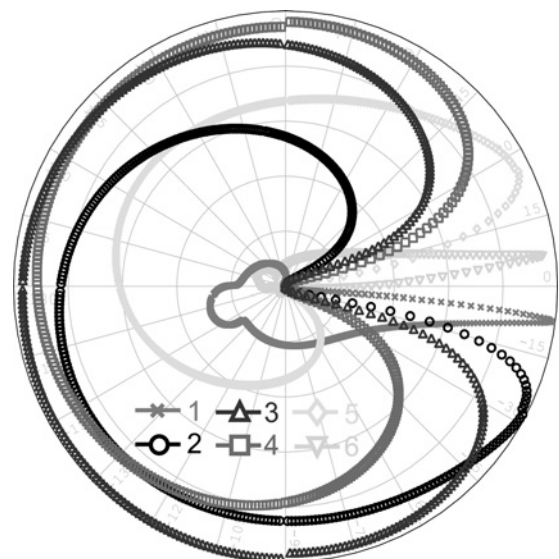


Fig. 3 S_{21} of the triple stub circuit topology for different values of t ($\alpha = 2$ Np/m @ 15 GHz): (1) $t = 0.02\lambda$, (2) $t = 0.0375\lambda$, (3) $t = \lambda/8$, (4) $t = 3\lambda/8$, (5) $t = 0.4625\lambda$, (6) $t = 0.49\lambda$

Without loss of generality, the input impedance is taken as Z_0 , which aims zero return loss. The change of the amplitude with zero reflection means that the power is dissipated within the circuit. This behaviour is worthy of examination because the circuit consists of only low-loss transmission lines (e.g. $R/\omega L = 0.033$ at 15 GHz, where R and L are the per unit length parameters of the transmission line). Indeed, resonance is the reason of the increasing loss of the circuit; adjusting the resonance parameters and consequent amplitude control are discussed in the following part.

3.1 Loss mechanism

In the triple stub circuit topology, there are three open-circuited terminations at the ends of the three stubs. In some certain frequencies where the path lengths between any two of these terminations that is, $x + y + t$, $y + z + t$, or $x + z + 2t$, become $n\lambda/2$, the circuit behaves as an open-circuited $\lambda/2$ resonator, which can be visualised in Figs. 4a–c. In these frequencies, loss of the circuit, which is defined as in (11), increases significantly because of the power coupled into the resonator.

$$L = \frac{|S_{21}|^2}{1 - |S_{11}|^2} \quad (11)$$

Fig. 5 shows loss of the circuit for three sample insertion phase/amplitude states as an example. For the (–7 dB, 45°) state, the loss graph has peaks at 8.06 and 15.08 GHz. The $x + y + t$, $y + z + t$ and $x + z + 2t$ totals for this state are equal to 20 042, 20 646 and 31 415 μm , which have electrical lengths equal to $\lambda/2$ at 7.48, 7.26 and 4.77 GHz, respectively. The peaks occur at frequencies that are very close to the first (7.48 GHz) and second (14.96 GHz) multiples of the $\lambda/2$ resonance. These calculations show that the triple stub circuit topology, which is composed of only low-loss transmission lines, can have high amounts of losses because of the open-circuited $\lambda/2$ resonators. Perturbation due to the transmission line losses may be the reason of the slight difference between the simulated resonance frequencies and the calculated ones.

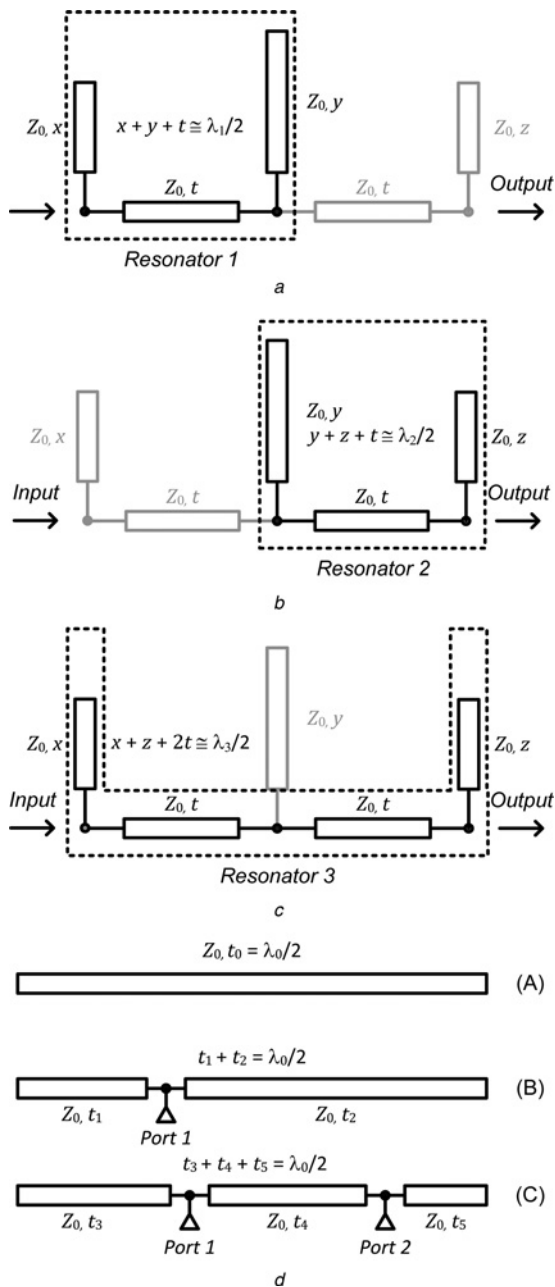


Fig. 4 Resonators in triple stub circuit topology
 a-c Open-circuited resonators in the triple stub circuit topology
 d $\lambda_0/2$ resonator with 0, 1 and 2 input/output ports

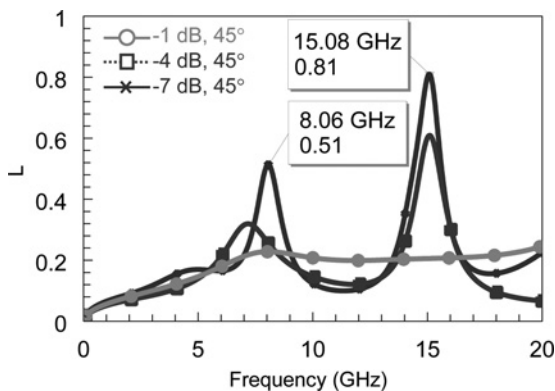


Fig. 5 Loss of the triple stub circuit topology when it is set to three sample insertion phase/amplitude states at 15 GHz

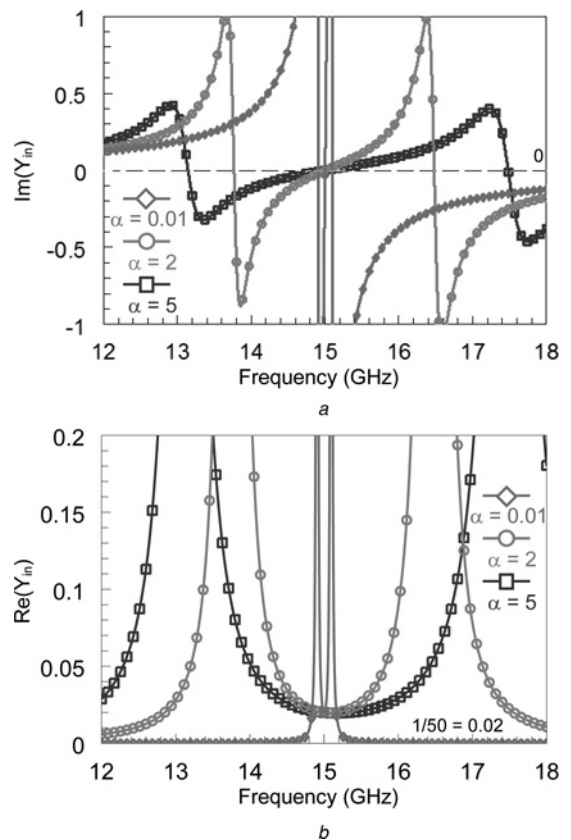


Fig. 6 Input admittance of the resonator circuit (B) where the input admittance of the circuit is set to Y_0

a Imaginary part of the input admittance of the resonator circuit (B)
 b Real part of the input admittance of the resonator circuit (B)

3.2 Amplitude control

Controlling the amplitude of the input signal can be explained by approaching the problem from the quality factor point of

Table 1 Parameters of circuit (B) and (C) that are used for the calculations

α , Np/m	Circuit (B)		Circuit (C)		
	t_1 , μm	t_2 , μm	t_3 , μm	t_4 , μm	t_5 , μm
0.01	4965	5028	4963	46.01	4984
2	4547	5446	4519	646.8	4827
5	4285	5708	4249	1015	4730

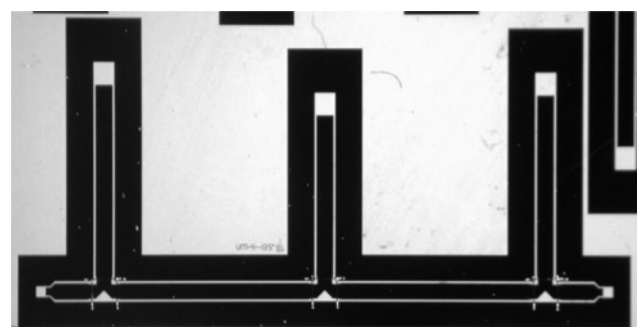
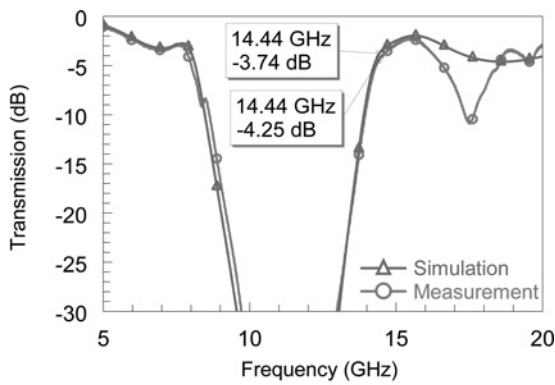
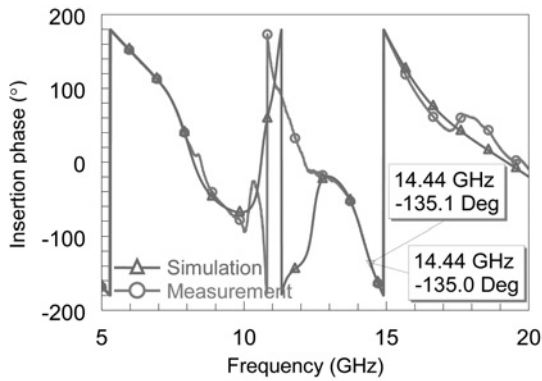


Fig. 7 Photograph of one of the fabricated triple stub insertion phase/amplitude control circuits

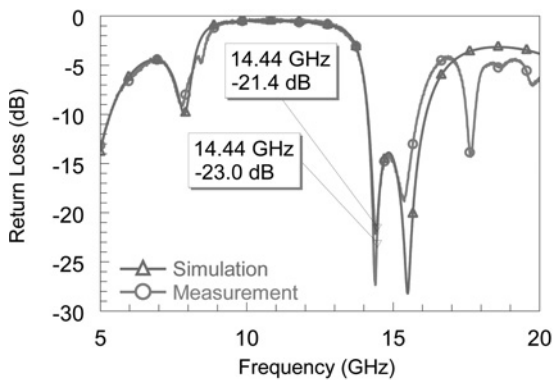
Circuit is designed for $(-4 \text{ dB}, -135^\circ)$ state, and it measures $13.4 \times 7 \text{ mm}$



a



b



c

Fig. 8 Measurement results of the triple stub circuit that is designed for $(-4 \text{ dB}, -135^\circ)$ state compared with the simulations

a Transmission coefficient, $|S_{21}|$

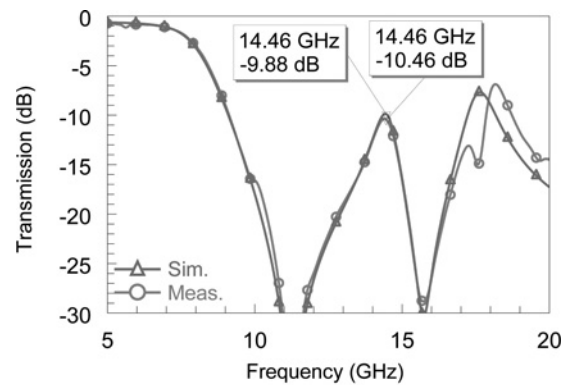
b Insertion phase, $\angle S_{21}$

c Return loss, $|S_{11}|$

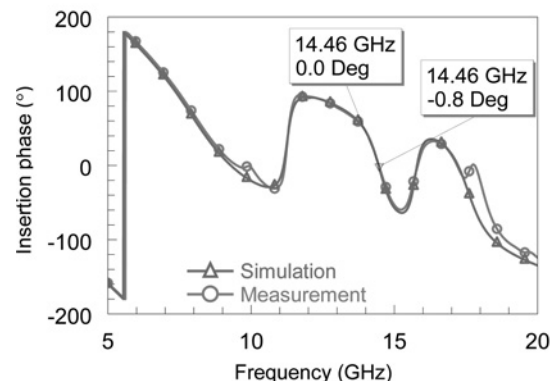
view. Let us consider the circuits given in Fig. 4d. Circuit (A) is an open-circuited $\lambda/2$ transmission line resonator, which behaves like a shunt resonant circuit around $f=f_0$. When this resonator is excited as in circuit (B), it is loaded by the impedance of port 1. As a result, the loaded quality factor, Q_L , which is given in (12), decreases significantly

$$\frac{1}{Q_L} = \frac{1}{Q} + \frac{1}{Q_e} \quad (12)$$

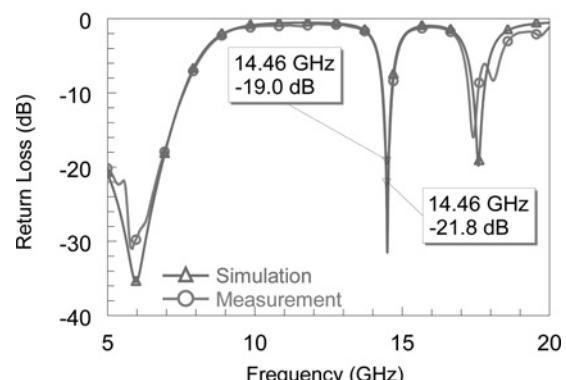
The input admittance looking into port 1 of circuit (B) is purely real because the imaginary parts of the admittances looking towards each direction cancel each other ($t_1 + t_2 = \lambda_0/2$). Hence, by changing the position of the port, that is, the excitation, within the resonator, the real part of the input admittance at port 1 can be easily set to



a



b



c

Fig. 9 Measurement results of the triple stub circuit that is designed for $(-9 \text{ dB}, 0^\circ)$ state compared with the simulations (a) $|S_{21}|$ (b) $\angle S_{21}$ (c) $|S_{11}|$

a Transmission coefficient, $|S_{21}|$

b Insertion phase, $\angle S_{21}$

c Return loss, $|S_{11}|$

$Y_0 = 1/Z_0$. This situation is true for ‘any value of non-zero transmission line attenuation constant’, α . This is demonstrated in Fig. 6 for different values of α . There always exists a point where the sum of the real parts of the admittances looking towards each direction is equal to Y_0 . This, as a result, means that the maximum power transfer to circuit (B) can be obtained for any given value of α .

By adding one more port as in circuit (C), some ratio of the input power can be taken out of the circuit. This ratio depends on the positions of the two ports within the $\lambda_0/2$ resonator. At the same time, the return loss at port 1 can still be kept equal to zero. A sample case for circuit (C) is presented, where t_3 , t_4 and t_5 are adjusted to have $|S_{21}| = -9 \text{ dB}$, which corresponds to a loss of $L = 0.875$, for different

values of α . The transmission line lengths that are used for the calculations are presented in Table 1.

Control of the circuit loss is actually achieved by adjusting the value of the external quality factor, Q_e , of the circuit. Arranging the positions of the input and output ports actually correspond to changing Q_e , which results as a change of Q_L , and this, consequently, means that the ratio of power that will be dissipated in the circuit can be controlled. The same behaviour can also be achieved 'by changing only the port impedances, Z_p , for any given positions of port 1 and port 2'. The only changing parameter in the latter case is the port impedance, Z_p , and it is related to Q_e as in (13)

$$Q_e = \frac{Z_p}{\omega_0 L} \tag{13}$$

This result makes it clear one more time that the output power is controlled by adjusting the Q_e of circuit (C).

3.3 Verification

Several analytical solution methods are used for developing explicit closed form equations in the presence of the losses. However, these methods yield four complex, transcendental equations including complex hyperbolic functions that are not appropriate for closed form equations. Nevertheless, the existence of the solutions is proven for a high number of insertion phase/amplitude states using optimisation and search of the whole solution space.

The instantaneous frequency bandwidth can be questioned when the triple stub circuit topology is employed for instantaneous insertion phase/amplitude control. The topology naturally has a narrowband response as it is a transmission line-based circuit. However, it has linear phase against frequency relation in an acceptable frequency range whereas this bandwidth is limited by the frequency dependence of its insertion loss. A sample case is presented here for quantitative investigation. The bandwidth for (-1 dB/ 45°) state centred at 15 GHz is 2.6 GHz considering flat insertion loss (± 0.2 dB for -1 dB), the return loss better than -15 dB and linear phase response. 2.6 GHz bandwidth corresponds to 17% bandwidth at 15 GHz, and it is limited by the return loss. The bandwidth of this triple stub circuit becomes narrower once it is set to lower amplitude states. For example, the instantaneous bandwidth for (-7 dB/ 45°) state is 260 MHz (1.7%), and it is again

limited by its return loss. The insertion phase response again shows linear phase against frequency relation where the amplitude remains within ± 1 dB range in this bandwidth. For higher amplitude levels, the instantaneous bandwidth is sufficient for most of the practical applications. Lower amplitude cases are given for demonstration purposes.

4 Experimental verification

The insertion phase/amplitude control using the triple stub circuit topology is experimentally verified by the implementation and measurements of some sample circuits that include several insertion phase/amplitude states.

The triple stub circuits are implemented using 50 Ω coplanar waveguides (CPWs). The dimensions of the CPW are $G/W/G = 36/378/36$ μm , which are calculated using the formulation given in [16]. The parameters that are used in the CPW design are $Z_0 = 50$ Ω , $\epsilon_{r, \text{eff}} = 2.36$, $\alpha = 52$ dB/m @ 15 GHz. The formulation gives $\alpha = 36$ dB/m attenuation constant; however, $\alpha = 52$ dB/m is used in the designs depending on the previous measurement experience [21], which is also confirmed by HFSS v10 simulations [22].

Fig. 7 shows a photograph of one of the fabricated single metal layer triple stub circuits. Thru-reflect-line (TRL) calibration is used in 5–20 GHz frequency band for the measurement of the circuits. The parameters of the CPW lines are extracted from the test structures that are fabricated on the same wafer. The extracted parameters for the CPW are $Z_0 = 50.4$ Ω , $\epsilon_{r, \text{eff}} = 2.43$ and $\alpha = 50$ dB/m @ 15 GHz. These values are very close to the design values except for a slight increase in $\epsilon_{r, \text{eff}}$. Figs. 8 and 9 show samples from the measurement results of the circuits designed for different insertion phase/amplitude states. Table 2 presents the comparison of the simulation and measurement results of all of the fabricated circuits.

Considering the responses given in Figs. 8 and 9, the measurement results are in very good agreement with the simulations. However, the desired performance is achieved at frequencies that are slightly lower than the centre design frequency, which is 15 GHz. This situation has two reasons. The first one is that the $\epsilon_{r, \text{eff}}$ used in the designs, 2.36, is lower than that of the measured one, 2.43. Therefore all of the CPWs are electrically longer than the simulated ones, and the desired performance normally shifts to the lower frequencies. The second reason is that it is hard to obtain a constant wirebond height with a manual wirebonder, which directly affects the electrical lengths of the stubs and

Table 2 Comparison of the simulation and measurement results of the fabricated triple stub circuits

Design no	Simulation			Measurement			Frequency, GHz
	S_{11}	S_{21}		S_{11}	S_{21}		
	Mg., dB	Mg., dB	Ph., deg	Mg., dB	Mg., dB	Ph., deg	
1	-287	-1	0	-15.3	-1.6	0	14.44
2	-281	-1	45	-28.2	-1.2	45	14.79
3	-280	-1	90	-28.4	-1.1	90	14.60
4	-281	-1	180	-24.8	-0.9	-179.9	14.55
5	-291	-3	-90	-12.7	-3.7	-90	14.69
6	-284	-4	-135	-23	-4.3	-135.1	14.44
7	-275	-6	90	-20.9	-5.6	90	14.64
8	-275	-7	135	-29	-5.2	128.2	14.70
9	-272	-9	0	-19	-10.5	-0.8	14.46
10	-278	-20	0	-12.7	-16	-7.9	14.43

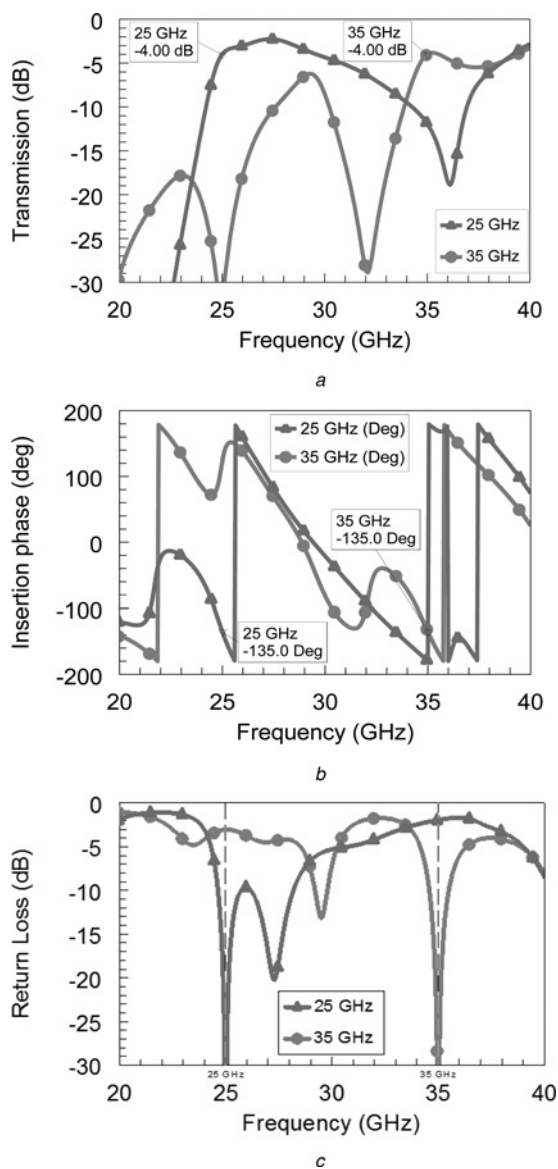


Fig. 10 Simulated performance of the triple stub circuits that are designed for $(-4 \text{ dB}, -135^\circ)$ state at selected sample frequencies for frequency reconfiguration

- a Transmission coefficient, $|S_{21}|$
 b Insertion phase, $\angle S_{21}$
 c Return loss, $|S_{11}|$

connecting transmission lines. However, when the measured thicknesses of the wirebonds are inserted in the simulations, a very good agreement is obtained as shown in the above figures.

In order to demonstrate the frequency reconfigurability of the triple stub circuit topology, two sample circuit designs are presented that are designed for $(-4 \text{ dB}, -135^\circ)$ state at two sample frequencies, which are 25 and 35 GHz. During the simulation of these circuits, the parameters that have been presented previously within this section are used. Fig. 10 shows the simulation results of both circuits. The simulation results clearly show that the circuit can be easily reconfigured to any selected random frequencies using the same parameters.

5 Conclusion

This paper presented a novel method for simultaneous insertion phase and amplitude control using triple stub

circuit topology. The insertion phase and amplitude control mechanisms were demonstrated from the analytical and numerical points of view. The method of controlling the amplitude using only low-loss transmission lines was investigated in detail. It was shown that the amount of the output power from a two-port, low-loss, $\lambda/2$ -long transmission line circuit can be controlled by adjusting its external quality factor. Simultaneous insertion phase and amplitude control ability of the triple stub circuit topology was also verified with the fabrication of ten CPW-based circuits, whose measurement results are in very good agreement with the simulations

The most important result presented in this paper is that a 'properly designed, reconfigurable triple stub circuit' may unify the functions of impedance transformation, amplitude control and insertion phase control circuits, which are crucial for most of the microwave applications. The triple stub circuit topology can be easily implemented as a 'reconfigurable circuit' with any state-of-the-art fabrication technologies such as monolithic microwave integrated circuits (MMIC) or MEMS. A reconfigurable triple stub circuit can be used in a wide range of applications, and the first candidate will be the phased arrays, which will result with increasing system performance and decreasing system complexity.

6 Acknowledgments

This work was supported by the Scientific and Technical Research Council of Turkey (TUBITAK-EEEAG-104E048) and the Turkish State Planning Organisation (DPT). The authors thank Mr Orhan Akar for his valuable guidance during the fabrication, Mr Halil Ibrahim Atasoy, Mr Cagri Cetintepe and Dr Kagan Topalli for their help. They also thank METU-MEMS Centre Fabrication personnel for their support.

7 References

- Parker, D., Zimmermann, D.C.: 'Phased arrays—part I: theory and architectures', *IEEE Trans. Microw. Theory Tech.*, 2002, **50**, (3), pp. 678–687
- Parker, D., Zimmermann, D.C.: 'Phased arrays—part II: implementations, applications, and future trends', *IEEE Trans. Microw. Theory Tech.*, 2002, **50**, (3), pp. 688–698
- Garver, R.V.: 'Broad-band diode phase shifters', *IEEE Trans. Microw. Theory Tech.*, 1972, **20**, (5), pp. 314–323
- White, J.F.: 'Diode phase shifters for array antennas', *IEEE Trans. Microw. Theory Tech.*, 1974, **22**, (6), pp. 658–674
- Little, W.A., Yuan, J., Snellings, C.C.: 'Hybrid integrated circuit digital phase shifters'. Proc. IEEE Int. Solid-State Circuits Conf., February 1967, pp. 58–59
- Aust, M., Wang, H., Carandang, R., *et al.*: 'GaAs monolithic components development for Q-band phased array application'. Proc. IEEE Int. Microw. Symp., Albuquerque, NM, USA, June 1992, pp. 703–706
- Battershall, B.W., Emmons, S.P.: 'Optimization of diode structures for monolithic integrated circuits', *IEEE Trans. Microw. Theory Tech.*, 1968, **16**, (7), pp. 445–450
- Jacomb-Hood, A.W., Seielstad, D., Merrill, J.D.: 'A three-bit monolithic phase shifter at V-band'. Proc. IEEE Microwave and Millimeter-Wave Monolithic Circuits Symp., June 1987, pp. 81–84
- White, J.F.: 'High power, p-i-n diode controlled, microwave transmission phase shifters', *IEEE Trans. Microw. Theory Tech.*, 1965, **13**, (2), pp. 233–242
- Murphy, T.A., Gipprich, J.W., Hines, M.E., Kruger, D.: 'A 6-bit GMIC phase shifter for 6–18 GHz'. Proc. IEEE Int. Microwave Symp., Albuquerque, NM, USA, June 1992, pp. 1171–1174
- Schindler, M.J., Miller, M.E.: 'A 3-bit K/Ka band MMIC phase shifter'. Proc. IEEE Microwave and Millimeter-Wave Monolithic Circuits Symp., New York, USA, 1988, pp. 95–98
- Opp, F.L., Hoffman, W.F.: 'Design of digital loaded-line phase-shift networks for microwave thin-film applications', *IEEE Trans. Microw. Theory Tech.*, 1968, **16**, (7), pp. 462–468

- 13 Davis, W.A.: 'Design equations and bandwidth of loaded-line phase shifters', *IEEE Trans. Microw. Theory Tech.*, 1974, **22**, (5), pp. 561–563
- 14 Bahl, L.J., Gupta, K.C.: 'Design of loaded-line p-i-n diode phase shifter circuits', *IEEE Trans. Microw. Theory Tech.*, 1980, **28**, (3), pp. 219–224
- 15 Atwater, H.A.: 'Circuit design of the loaded-line phase shifter', *IEEE Trans. Microw. Theory Tech.*, 1985, **33**, (7), pp. 626–634
- 16 Simons, R.: 'Coplanar waveguide circuits, components, and systems' (John Wiley & Sons, 2001)
- 17 Vähä-Heikkilä, T., Varis, J., Tuovinen, J., Rebeiz, G.M.: 'W-band RF MEMS double and triple-stub impedance tuners'. Proc. IEEE Int. Microw. Symp., Long Beach, CA, USA, June 2005, pp. 12–17
- 18 Unlu, M., Topalli, K., Atasoy, H.I., *et al.*: 'A reconfigurable RF MEMS triple stub impedance matching network'. Proc. 36th European Microwave Conf., Manchester, UK, September 2006, pp. 1370–1373
- 19 Vähä-Heikkilä, T., Van Caekenberghe, K., Varis, J., Tuovinen, J., Rebeiz, G.M.: 'RF MEMS impedance tuners for 6–24 GHz applications', *Int. J. RF Microw. CAE*, 2007, **17**, (3), pp. 265–278
- 20 Microwave Office 2006 'Applied wave research Inc' (El Segundo, CA, 2006)
- 21 Unlu, M.: 'Novel impedance tuner, phase shifter and vector modulators using RF MEMS technology'. PhD thesis, Middle East Technical University, 2009
- 22 HFSS v10 'Ansoft corporation' (Pittsburgh, PA, USA, 2002)